High Gain Hybrid Graphene-Organic Semiconductor Phototransistors

Huisman, Everardus H.; Shulga, Artem G.; Zomer, Paul J.; Tombros, Nikolaos; Bartesaghi, Davide; Bisri, Satria Zulkarnaen; Loi, Maria A.; Koster, L. Jan Anton; van Wees, Bart J.

Published in:
ACS Applied Materials & Interfaces

DOI:
10.1021/acsami.5b00610

Publication date:
2015

ACS APPLIED MATERIALS & INTERFACES

Research Article

www.acsami.org

High Gain Hybrid Graphene–Organic Semiconductor Phototransistors

Everardus H. Huisman,*[,†,‡] Artem G. Shulga,[†] Paul J. Zomer,[†,‡] Nikolaos Tombros,[†] Davide Bartesaghi,[†,§] Satria Zulkarnaen Bisri,[†] Maria A. Loi,[†] L. Jan Anton Koster,[†] and Bart J. van Wees[†]

[†]Zernike Institute for Advanced Materials, University of Gronigen, Nijenborgh 4, 9747 AG Groningen, The Netherlands

[‡]Stichting Fundamenteel Onderzoek der Materie, P.O. Box 3021, 3502 GA Utrecht, The Netherlands

[§]Dutch Polymer Institute, P.O. Box 902, 5600 AX Eindhoven, The Netherlands

Supporting Information

ABSTRACT: Hybrid phototransistors of graphene and the organic semiconductor poly(3-hexylthiophene-2,5-diyl) (P3HT) are presented. Two types of phototransistors are demonstrated with a charge carrier transit time that differs by more than 6 orders of magnitude. High transit time devices are fabricated using a photoresist-free recipe to create large−area graphene transistors made out of graphene grown by chemical vapor deposition. Low transit time devices are fabricated out of mechanically exfoliated graphene on top of mechanically exfoliated hexagonal boron nitride using standard e-beam lithography. Responsivities exceeding 10^5 A/W are obtained for the low transit time devices.

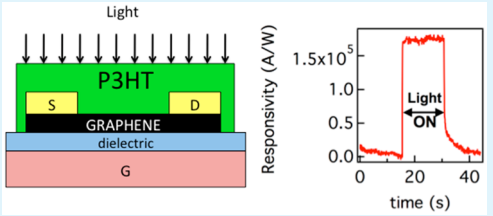

KEYWORDS: *graphene, organic electronics, organic semiconductors, photodetectors, phototransistors, photoconductivity*

INTRODUCTION

Graphene and all-graphene devices hold great promise for optoelectronics due to its unique combination of optical, mechanical and electronic properties.[1,2] However, the sensitivity of graphene light-sensing devices is limited since a single layer of graphene only absorbs 2.3% of light over a wide spectral range. A way out is to integrate graphene devices with light-absorbing materials. Recently, it has been demonstrated that the external responsivity of a graphene field-effect transistor can be highly improved by integrating semiconducting materials on top of a graphene channel.[3,4] These devices form a new class of photodetectors with a relatively high sensitivity not described in classic textbooks on photoconductors.[5,6] Semiconducting materials explored for this purpose include CdSe colloidal quantum dots,[7] PbS colloidal quantum dots,[8−11] ZnO quantum dots,[12,13] graphite quantum dots,[14] TiO_2 nanopoarticles,[15] Al_2O_3 thin films,[16] MoS_2 (ultrathin) layers,[17−20] chlorophyll molecules,[21] and C60 molecules.[22] Organic semiconductors form a particularly attractive class of semiconductors since their physical properties can be tuned chemically.[23] Furthermore, hybrid graphene-organic semiconductor devices are expected to be promising for large-area, flexible, transparent and low-cost electronics. Surprisingly, their use in graphene-based optoelectronic devices is relatively unexplored, although organic semiconductors have for example been reported when studying photo desorption of oxygen on graphene,[24] the photo response of an organic bulk heterojunction phototransistor,[25] the photo response of P3HT-PbS quantum dots phototransistors[26] and the photo response of composite materials made out of chemically converted graphenes and water-soluble polymers.[27] To the best of our knowledge, hybrid graphene-organic semiconductors phototransistors with a high gain have not been reported. In this Letter, we report hybrid graphene-organic semiconductors phototransistors using poly(3-hexylthiophene-2,5-diyl) (P3HT), a well-characterized organic semiconductor.[23] Two sources of graphene are utilized to fabricate hybrid graphene-P3HT phototransistors: graphene on silicon/silicon dioxide grown by chemical vapor deposition (CVD) and mechanically exfoliated graphene on top of mechanically exfoliated hexagonal Boron Nitride (BN). Large-area transistors are patterned from CVD graphene using a photoresist-free recipe, while mechanically exfoliated graphene on BN is used to fabricate transistors of only a few microns in length. Hence, two types of hybrid graphene-P3HT transistors with a distinctly different carrier transit time are presented. It is demonstrated that solution-processable organic semiconductors can be used to obtain high gain phototransistors with responsivities exceeding 10^5 A/W for low transit time graphene devices.

Let us review the basic device operation. Figure 1a shows a device schematic of a hybrid graphene-semiconductor phototransistor. In this device, the current in a graphene channel of length L and width W is monitored while applying a bias voltage V_{sd} between a source (S) and drain (D) electrode and a voltage V_g to the gate electrode (G) which is separated from the channel by an insulating dielectric. The full channel is exposed to a light source of wavelength λ with a homogeneous power density P. The rate of photons reaching the channel

Received: September 10, 2014
Accepted: May 11, 2015
Published: May 11, 2015

DOI: 10.1021/acsami.5b00610
ACS Appl. Mater. Interfaces 2015, 7, 11083−11088

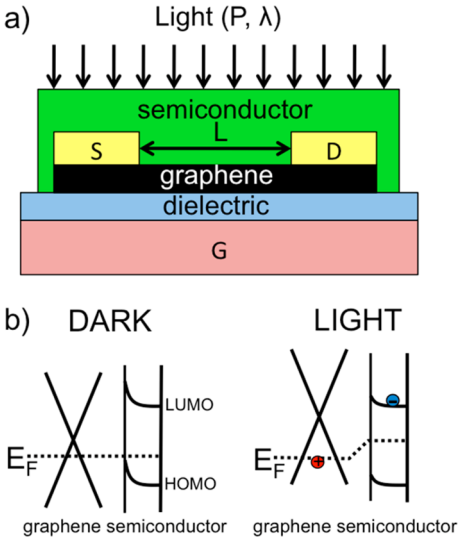

Figure 1. (a) Side view of a hybrid graphene-semiconductor device showing a channel of length L connected to source (S) and drain (D) electrodes on top of an insulating dielectric substrate connected to a gate electrode (G). The device is illuminated by a homogeneous light-source of wavelength λ and power density P. (b) Schematic of a graphene P3HT interface in the dark and under light exposure. The electronic structure of graphene is represented by a double cone structure filled with charge carriers up to the Fermi level (E_F). P3HT is represented by a HOMO and a LUMO level. Exposing the interface to light leads to nonequilibrium n-doping of the semiconductor with corresponding nonequilibrium p-doping of the graphene, resulting in a change of the conductivity of graphene.

surface is then given by, $F = [(PWL\lambda)/(hc)]$ where h is Planck's constant and c is the speed of light. When light is absorbed by the semiconductor, graphene's conductivity changes. In recent literature this is often explained in terms of a light-induced gating field because of rearrangement of charges close to the graphene semiconductor interface. Figure 1b shows a schematic of an interface between graphene and a thin layer of a p-type semiconductor (P3HT is a p-type semiconductor with $E_{HOMO} = -4.9$ eV[28] and $E_{LUMO} = -3.0$ eV[28]) both in the dark and under light exposure. Graphene's intrinsic Fermi level is located at its charge neutrality point ($E_F = -4.6$ eV).[29] However, in practice we find that graphene is doped because of interactions with its environment. Due to alignment of the Fermi levels in both materials, a built-in electric field is present in the semiconductor near the interface. Exposing the interface to light leads to nonequilibrium n-doping of the semiconductor with corresponding nonequilibrium p-doping of the graphene, resulting in a change of the conductivity of graphene.

To read-out the light-induced conductivity change of the graphene channel, the lifetime τ of the induced carriers in graphene needs to be longer than the transit time of a charge carrier to cross the graphene channel $\tau_{tr} = [L^2/(\mu V_{sd})]$. Here, μ is the mobility of charge carriers in graphene. The high gain reported for hybrid semiconductor-graphene phototransistors can be understood when drawing the analogy with bulk semiconductor phototransistors. When assuming that every exciton yields a mobile carrier in the graphene, the photo-induced current is simply given by $I = eFG$.[5] Here G is the photoconductive gain $G = (\tau/\tau_{tr})$. This simplified picture shows that high gain is obtained by decreasing τ_{tr} or by increasing τ. Furthermore, the responsivity of the phototransistor is given by $R = [(I/(PLW)] = [(e\lambda)/(hc)](\tau/\tau_{tr}) = [(e\lambda)/(hc)][(\tau\mu V_{sd})/$

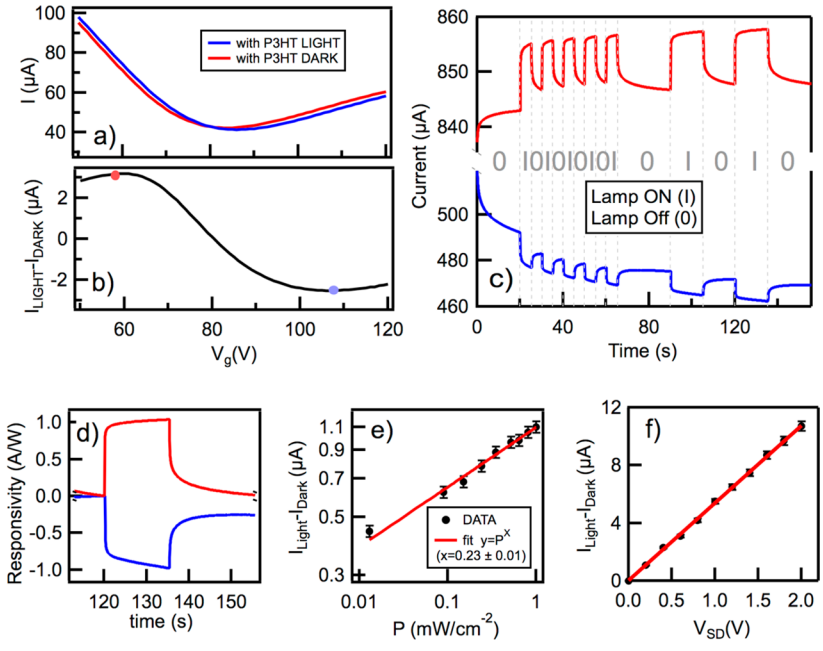

Figure 2. (a) Transfer characteristics (source-drain current versus gate voltage) of a graphene field-effect transistor made out of CVD graphene on silicon dioxide ($L = W = 1$ mm, $V_{SD} = 0.2$ V) in the dark (red) and when illuminating the entire channel with a lamp (blue, $\lambda = 500$ nm, $P = 0.97$ mW cm^{-2}). (b) Light-induced current obtained by subtracting the two curves of Figure 2a ($I_{LIGHT} - I_{DARK}$). (c) Transient measurements at two distinct gate voltages, $V_{SD} = 2$ V, $V_G = 58$ V (red line) and $V_G = 108$ V (blue line). The lamp is switched on at $t = 20$, 30, 40, 50, 60, 90, and 120 s and switched off at 25, 35, 45, 55, 65, 105, and 135 s. (d) Zoom in of the last part of Figure 2c. The responsivity is obtained by subtracting the current recorded at $t = 120$ s from the data and dividing the resulting induced photocurrent by the total applied light power to the channel surface. (e) Log–log plot of the light-induced current as a function of light power density. (f) Light-induced current as a function of bias voltage.

DOI: 10.1021/acsami.5b00610
ACS Appl. Mater. Interfaces 2015, 7, 11083–11088

$(L^2)]$ and scales with the inverse of the transit time of the carriers in the graphene channel. As we will show below, the transit time is easily controlled over orders of magnitude by modifying the channel length of the device.[30] Also, the reported high gain for graphene-based phototransistors can now be understood since these devices benefit from graphene's high mobility and a high lifetime of the light-induced carriers.

RESULTS AND DISCUSSION

To test whether organic semiconductors can be used to obtain graphene-based phototransistors in experiment, we utilize a simple photoresist-free approach to fabricate large-area CVD graphene transistors. For technical details of the approach we refer to ref 31. In brief, a graphene channel of width W = 1.0 mm and length L = 1.0 mm is defined on commercially available single layer graphene on 300 nm silicon dioxide obtained from Graphenea using a photoresist-free lithographic process.[31] Devices are loaded in a high vacuum probe station (5×10^{-7} mbar) equipped with a heater and annealed overnight at 120 °C. After they were cooled down to room temperature, these "graphene-only" devices are characterized with a Keithley 4200-SCS with four Source Meter Units. Subsequently, devices are taken out of the probe station and a fresh solution of P3HT in chloroform (Rieke specialty polymers 4002-EE, 7 mg/mL stirred overnight) is spin-coated in air at 3000 rpm. The resulting layer was measured to be 55 nm. Directly after spin-coating, the device is loaded into high vacuum and reannealed overnight at 120 °C. After they were cooled down to room temperature, the devices are analyzed again.

The red curve in Figure 2a shows the transfer curve of a typical device (device I) in the dark. Typically a small hysteresis between the trace and retrace is observed for field-effect transistors made out of CVD graphene (see Figure S1 in the Supporting Information). In the following, only the trace part is analyzed and the sweeprate is kept constant. To extract a characteristic mobility and the position of the charge neutrality point, a fit procedure described in the Supporting Information is used. From the best fit a mobility of $\mu = (1.54 \pm 0.01) \times 10^3$ $cm^2\ V^{-1}\ s^{-1}$ is obtained and is found to be similar to the mobility obtained for the pristine device ($\mu = (1.52 \pm 0.01) \times 10^3$ $cm^2\ V^{-1}\ s^{-1}$). This shows that the presence of P3HT does not significantly alter the mobility of charge carriers in these graphene devices. The charge neutrality point is reached at a gate voltage of $V_{CNP} = (80.2 \pm 0.1)$ V. This is substantially higher than the position of the charge neutrality point of the pristine device (V_{CNP}= (56.3 ± 0.1) V). An identically processed device showed similar results (device II, without P3HT layer $V_{CNP} = (53.5 \pm 0.1)$ V, $\mu = (1.41 \pm 0.01) \times 10^3$ $cm^2\ V^{-1}\ s^{-1}$. With P3HT layer: $V_{CNP} = (78.6 \pm 0.1)$ V, $\mu = (1.59 \pm 0.01) \times 10^3$ $cm^2\ V^{-1}\ s^{-1}$).

After application of P3HT and characterization of the device in the dark, the devices are homogeneously illuminated over the entire chip through the viewing window of the probe station using a 150W solar simulator (Newport 92259−1000) equipped with a 2 in. calibrated 500 nm Scott bandpass filter. The power density of the lamp with bandpass filter is determined to be 9.7×10^{-4} W/cm^2 using a silicon standard reference cell. The blue curve in Figure 2a shows the corresponding transfer curve for device I when the lamp is turned on. When switching on the lamp a shift in the position of the charge neutrality point of $\Delta V_g = 0.9 \pm 0.2$ V and $\Delta V_g = 1.7 \pm 0.2$ V is obtained for device I and II, respectively. This corresponds with an induced charge carrier density $\Delta n = (6.5 \pm 1.4) \times 10^{10}$ cm^{-2} and $\Delta n = (12.2 \pm 1.4) \times 10^{10}$ cm^{-2}, respectively. Figure 2b displays the light-induced current as a function of gate voltage and is obtained by subtracting the transfer curve in the dark from the transfer curve when the lamp is turned on. This difference curve is similar to the derivative of the transfer curve itself indicating that the applied light can be interpreted as a gating field ΔV_g, $I_{LIGHT} - I_{DARK} \propto \Delta V_g[(dI)/(DV_g)]$. It is also important to note that the light-induced response can be reversed in sign and can even be switched off electrically by tuning the Fermi level in graphene using the gate electrode.

Figure 2c shows transient measurements while switching the lamp on and off at specific times using a shutter. At t = 0 s, the gate voltage is switched to a set value close to the inflection point of the transfer curve (as indicated by the red and blue dot in Figure 2b). This sudden gate stress results in a drift in the current. A similar drift is also present in graphene only devices and indicates that the graphene still interacts with other electronic states at a relatively slow rate. Figure 2d shows a zoom-in after the drift has mostly saturated. Interestingly, there is an asymmetry in the response between switching the lamp from OFF to ON and switching the lamp from ON to OFF. When switching from OFF to ON, 90% of the induced photocurrent is obtained within 60 ms (limited by the time resolution of the experiment). However, when switching from ON to OFF a slower time response is observed. The experimental data can be fitted using a double exponential decay function, $I = I_0 + A_1 \exp[(t - t_0)/\tau_1] + A_2 \exp[(t - t_0)/\tau_2]$ with τ_1 = 0.15 s, τ_2 = 5.1 s, and A_1/A_2 = 1.6 at the electron side (V_g = 58 V) and τ_1 = 0.17 s, τ_2 = 2.9 s, and A_1/A_2 = 1.5 at the hole side (V_g = 108 V). Note that the time scales obtained are still substantially lower than the expected transit time of charge carriers in the P3HT to cross a channel of 1 mm in length (~1000 s, assuming a mobility of 1×10^{-4} $cm^2\ V^{-1}\ s^{-1}$). Therefore, it is unlikely that the observed slow response from ON to OFF is due to carriers traveling through the P3HT. The asymmetry in response is also observed for PbS colloidal quantum dot-graphene hybrid phototransistors.[8,9] For graphene only (without P3HT), no step in the current could be resolved when switching on the lamp within the measurement resolution of the electronics, meaning that the light-induced current change is <0.1% of the channel current (see Figure S4 in the Supporting Information).

Figure 2e shows the dependence of the photoinduced current with light power density P. P is controlled using a set of neutral density filters. The light-induced current is found to scale with the light power density P as $I_{LIGHT} - I_{DARK} \propto P^x$. A power $x = 0.23 \pm 0.01$ is extracted by fitting the data. Note that a similar powerlaw dependence (x = 0.24) of the photoinduced current with light power density is observed by Sun et al. for hybrid graphene-PbS phototransistors.[9] Figure 2f shows the dependence of the photoinduced current with applied source drain bias. As expected, a linear dependence of the photo-induced current is observed.

Table 1 summarizes the device dimensions, the mobility, the resulting transit time, the observed responsivity at V_{sd} = 200 mV and lifetime of the light-induced carriers for these "high" transit time CVD graphene devices. The lifetime of the light-induced carriers, $\tau = [(hcRL^2)/(e\lambda\mu V_{sd})]$ (see Introduction) is obtained using the measured responsivity and the mobility obtained from fitting the transfer curve in the dark. Note that this lifetime is not corrected for optical losses due to unabsorbed photons or due to absorbed photons that do not

DOI: 10.1021/acsami.5b00610
ACS Appl. Mater. Interfaces 2015, 7, 11083−11088

Table 1. Experimental Results of "High" Transit Time Hybrid CVD Graphene–P3HT Phototransistor Devices on Silicon Dioxide[a]

	CVD graphene on SiO_2	
	device I	device II
W (μm)	$(1.00 \pm 0.01) \times 10^3$	$(1.00 \pm 0.01) \times 10^3$
L (μm)	$(1.00 \pm 0.01) \times 10^3$	$(1.00 \pm 0.01) \times 10^3$
μ ($cm^2\ V^{-1}\ s^{-1}$)	$(1.54 \pm 0.01) \times 10^3$	$(1.59 \pm 0.01) \times 10^3$
τ_{tr} (ns)	$(3.3 \pm 0.1) \times 10^4$	$(3.1 \pm 0.1) \times 10^4$
R (A/W) (V_{sd} = 200 mV)	$(1.1 \pm 0.1) \times 10^{-1}$	$(1.6 \pm 0.1) \times 10^{-1}$
τ (μs)	9.0 ± 0.1	12.5 ± 0.1

[a]All data is obtained using a light source with a band pass filter (λ = 500 nm) with a constant power density (P = 0.97 mW cm^{-2}). Responsivities are obtained from transient measurements at a gate voltage at the inflection point of the transfer curve of a phototransistor in the dark at a bias voltage of 200 mV.

result in an exciton and can be seen as a lower bound of the actual lifetime of light-induced carriers in graphene. The measurements indeed confirm relatively long lifetimes of the induced charge carriers in graphene. However, due to the relatively high transit time these devices do not result in high responsivities (R = $(1.1 \pm 0.1) \times 10^{-1}$ A/W and R = $(1.6 \pm 0.1) \times 10^{-1}$ A/W, obtained at V_{sd} = 200 mV).

To verify whether the responsivities of hybrid graphene–P3HT devices indeed inversely scale with the transit time of the carriers in graphene, we fabricated field-effect transistors out of mechanically exfoliated graphene on top of mechanically exfoliated hexagonal boron nitride (BN) on a silicon dioxide wafer. These devices feature a higher charge carrier mobility than (mechanically exfoliated) graphene on a silicon dioxide wafer and a relatively short channel length.[32] Details of the processing can be found elsewhere.[32] In short, flakes of exfoliated multilayer BN on a 300 nm SiO_2 wafer are selected based on their optical contrast. Subsequently, graphene is mechanically exfoliated on top of a transparent polymer substrate attached to a custom prepared optical mask. Single-layer graphene flakes are selected based on their optical contrast using an optical microscope in reflection mode. The selected graphene flake is aligned on top of a selected BN flake using a modified maskaligner equipped with a heater in the stage. By making hard contact between the mask and the BN sample, intimate contact between the graphene and BN polymer substrate (holding the graphene flake) and the silicon dioxide (holding the BN flake) is realized. Heating the stage above the glass transition temperature of the polymer allows to remove the polymer layer from the mask, after which the polymer is removed by dissolving it in acetone. An atomic force microscopy (AFM) image of the graphene flake on top of BN is given in Figure S5 of the Supporting Information. The thickness of the BN was determined to be 25 ± 0.5 nm using AFM. Next, contacts are defined and deposited using standard e-beam lift-off lithography and e-beam vacuum metal evaporation (5 nm Ti, 75 nm Au). After lift-off, devices are annealed for 12 h at 330 °C in a furnace in a flow of Ar/H_2 (85%:15%) to remove residual polymer. An AFM image of the graphene flake on top of BN after annealing is given in Figure S6 of the Supporting Information.

Figure 3a shows a microscope image of a finished device showing two graphene regions between three contacts. The dimensions of the flakes are determined using optical microscopy and atomic force microscopy (see Table 2). Prior

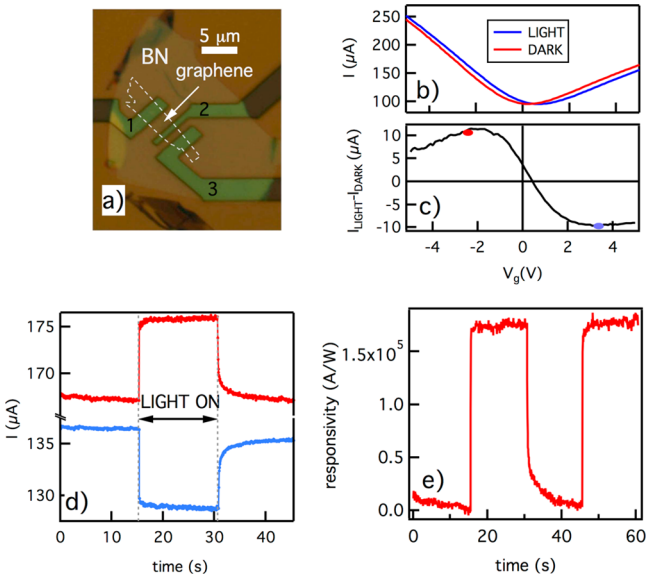

Figure 3. (a) Microscope image of a hybrid graphene–P3HT device made out of mechanically exfoliated graphene on top of hexagonal boron nitride (b) Transfer characteristics (source-drain current versus gate voltage) of the graphene channel between contact 1 and contact 2 (V_{SD} = 0.2 V) in the dark (red) and when illuminating the entire channel with a lamp (blue, λ = 500 nm, P = 0.97 mW cm^{-2}). (c) The light-induced current is obtained by subtracting the two curves of Figure 3b. (d) Current versus time measurements (V_{sd} = 0.2 V) of the region between contact 1 and 2 at two distinct gate voltages, V_G = −2.7 V (red line) and V_G = 3.3 V (blue line) when switching on and off the lamp. (e) Responsivity versus time of the region between contact 2 and 3. The responsivity is obtained by subtracting the current recorded at t = 15 s from the data and dividing the resulting induced photo current by the total applied power to the channel surface. The lamp is switched on at t = 15 and 45 s and switched off at t = 30 s.

Table 2. Experimental Results of "Low" Transit Time Hybrid Graphene–P3HT Phototransistor Devices Made out of Mechanically Exfoliated Graphene on Hexagonal Boron Nitride[a]

	exfoliated graphene on hBN	
	device I (BN12)	device II (BN23)
W (μm)	3.48 ± 0.01	3.97 ± 0.01
L (μm)	3.09 ± 0.01	1.46 ± 0.01
μ ($cm^2\ V^{-1}\ s^{-1}$)	$(2.56 \pm 0.01) \times 10^4$	$(1.65 \pm 0.01) \times 10^4$
τ_{tr} (ns)	$(1.86 \pm 0.05) \times 10^{-2}$	$(0.65 \pm 0.05) \times 10^{-2}$
R (A/W) (V_{sd} = 200 mV)	$(0.84 \pm 0.05) \times 10^5$	$(1.74 \pm 0.05) \times 10^5$
τ (μs)	3.9 ± 0.1	2.8 ± 0.1

[a]All data is obtained using a light source with a band pass filter (λ = 500 nm) with a constant power density (P = 0.97 mW cm^{-2}). Responsivities are obtained from transient measurements at a gate voltage at the inflection point of the transfer curve of a phototransistor in the dark at a bias voltage of 200 mV.

to spin-coating P3HT on top of the devices, devices are wire bonded, loaded in high vacuum (1.10^{-7} mbar) and analyzed. The hysteresis between the trace and retrace of a transfer curve for the mechanically exfoliated graphene on BN devices is found to be negligible. For the region between contacts 1 and 2 a mobility μ = $(9.70 \pm 0.08) \times 10^3$ $cm^2\ V^{-1}\ s^{-1}$ is obtained from the fit and the charge neutrality point is reached at a gate

DOI: 10.1021/acsami.5b00610
ACS Appl. Mater. Interfaces 2015, 7, 11083–11088

voltage V_g = (−1.19 ± 0.02) V.[33] For the region between contact 2 and 3 a mobility μ = (6.14 ± 0.06) × 10^3 cm^2 V^{-1} s^{-1} is obtained from the fit and the charge neutrality point is reached at a gate voltage V_g = (−1.43 ± 0.01) V. After characterization of the graphene-only device, the wire bonds are removed and a fresh solution of P3HT is spin-coated as described above and devices are reannealed at 120 °C in high-vacuum.

Figure 3b shows the transfer curve of the region between contact 1 and 2 in the dark and when the light is on. Interestingly, after spin-coating P3HT and reannealing in high-vacuum, the mobility of carriers in graphene is found to increase with respect to the same region before spin-coating P3HT. For the region between contact 1 and 2 a mobility of μ = (2.56 ± 0.01) × 10^5 cm^2 V^{-1} s^{-1} is obtained. Since the mobilities found before spin-coating are lower than typical values obtained for mechanically exfoliated graphene on top of BN,[32] we speculate that spin-coating P3HT and reannealing the hybrid device might have removed part of the scatterers present before spin-coating P3HT. Like in the case of the CVD graphene devices, a higher gate voltage needs to be applied after spin-coating P3HT and reannealing in order to reach the charge neutrality point (V_{CNP} = (0.14 ± 0.01) V). A similar increase in mobility and shift in the position of the charge neutrality point is observed for the region between contact 2 and 3 after spin-coating: μ = (1.65 ± 0.01) × 10^5 cm^2 V^{-1} and V_{CNP} = (0.41 ± 0.02) V.

Switching on the lamp resulted in a shift in the position of the charge neutrality point of (0.39 ± 0.02) V (region between contact 1 and 2) and 0.26 ± 0.04 V (region between contact 2 and 3). This corresponds to an induced charge carrier density Δn of (2.8 ± 0.1) 0 × 10^{10} cm^{-2} and (1.9 ± 0.2) × 10^{10} cm^{-2}, respectively. The characteristic sigmoidal curve displaying the gate tunability of the photoinduced current is again obtained when subtracting the two curves (Figure 3c).

Interestingly, the photoinduced charge carrier density is between two to six times lower than observed for high transit time devices discussed above. This suggests that the photo-induced doping of graphene is less efficient. Nevertheless, the induced photocurrent at the inflection point at a bias voltage of 200 mV in these low transit time devices is around four times higher compared to the high transit time devices.

Figure 3d and e shows transient measurements. Note there is no slow gate-stress response when suddenly switching on the gate voltage at t = 0. However, like in the case of the high transit time devices described above made out of CVD-grown graphene, an asymmetry in response between switching from OFF to ON and from ON to OFF is observed. While switching from OFF to ON, 90% the total light-induced current is realized within the time resolution of the experiment (60 ms). However, when switching from ON to OFF, the response is much slower. Like in the case of the high transit time devices, the data in Figure 3d is fitted using a double exponential decay function: τ_1 = 0.12 s, τ_2 =2.9 s, and A_1/A_2 = 1.5 at the electron side (V_g = −2.2 V) and τ_1 = 0.13 s, τ_2 =2.8 s, and A_1/A_2 = 1.5 at the hole side (V_g = 2.8 V). Note that these values are similar to the values obtained by fitting the high transit time devices. Also note that the time constants obtained are now substantially higher than the expected transit time of charge carriers in the P3HT to cross a channel of a few micron in length (∼1 ms, assuming a mobility of 1 × 10^{-4} cm^2 V^{-1} s^{-1}). Therefore, like in the case of the high transit time devices, also for these small scale devices it seems unlikely that the observed slow response from ON to OFF is due to carriers traveling through the P3HT.

Figure 3e shows the responsivity versus time for the shortest channel while switching the lamp on and off (region between contact 2 and 3, V_{sd} = 200 mV, at the inflection point of the transfer curve in the dark). Table 2 summarizes the relevant parameters for the low transit time devices. Most importantly, the data confirms that the responsivity scales with the inverse of the transit time, resulting in a responsivity of 1.74 × 10^5 A/W (λ = 500 nm) at a bias voltage of 200 mV for the channel with the shortest transit time.

The lifetime of the charge carriers in the graphene is found to be within the same order of magnitude for both types of devices. Still, for the low transit time devices τ is found to be roughly three times smaller than τ obtained for the high transit time devices which is consistent with the observed difference in the light-induced carrier density between both types of devices. This indicates that the light-induced carrier injection into the graphene is less efficient in the case of the low transit time devices. We speculate that differences in processing conditions between both types of devices are responsible for the remaining difference in the light-induced carrier density Δn and resulting lifetime of these carriers τ. To elucidate this, it is recommended to pattern graphene devices with an identical technology with a varying channel length. Furthermore, note that the obtained lifetimes for hybrid graphene−P3HT phototransistors are substantially lower than the lifetimes for light-induced carriers suggested by Konstantatos et al. for graphene-PbS photo-transistors at relatively low light intensities (τ = 20 ms for a gain of 10^7 A/W).[8] Part of this difference can be understood by differences in the optical absorption of colloidal quantum dots and organic semiconductors. It is interesting to investigate which other factors account for this difference.

CONCLUSION

In conclusion, hybrid phototransistors of graphene and the organic semiconductor P3HT have been demonstrated. Reducing the transit time of charge carriers in graphene by reducing the channel length and increasing the mobility optimized the photoconductive gain of these devices. Responsivities exceeding 10^5 A/W are obtained for hybrid graphene−P3HT devices out of mechanically exfoliated graphene on top of boron nitride.

ASSOCIATED CONTENT

Supporting Information

Trace and retrace in transfer curves of CVD graphene devices, fit procedure to obtain a mobility from a transfer curve, light response of a graphene only device, and atomic force microscopy images of the mechanically exfoliated flake on h-BN before and after annealing. The Supporting Information is available free of charge on the ACS Publications website at DOI: 10.1021/acsami.5b00610.

AUTHOR INFORMATION

Corresponding Author

*E-mail: eekhuisman@gmail.com.

Author Contributions

The manuscript was written through contributions of all authors. All authors have given approval to the final version of the manuscript.

DOI: 10.1021/acsami.5b00610
ACS Appl. Mater. Interfaces 2015, 7, 11083−11088

Funding

E.H.H. and P.J.Z. acknowledge the financial support of Stichting Fundamenteel Onderzoek der Materie. N.T. acknowledges the financial support of the Zernike Institute for Advanced Materials. A.G.S., S.Z.B., and M.A.L. acknowledge the financial support of the European Research Council (ERC) Starting Grant (No. 306983) "Hybrid solution processable materials for optoelectronic devices" (ERC-HySPOD).

Notes

The authors declare no competing financial interest.

■ ACKNOWLEDGMENTS

The authors thank Jan Harkema, Martijn de Roosz, Arjen Kamp, Niels van der Kaap, and Mark Speirs for their technical support and Stijn Goossens for useful discussions.

■ REFERENCES

(1) Bonaccorso, F.; Sun, Z.; Hasan, T.; Ferrari, A. C. Graphene Photonics and Optoelectronics. *Nat. Photonics* **2010**, *4*, 611−622.

(2) Withers, F.; Bointon, T. H.; Craciun, M. F.; Russo, S. All-Graphene Photodetectors. *ACS Nano* **2013**, *7*, 5052−5057.

(3) Sun, Z.; Chang, H. Graphene and Graphene-Like Two-Dimensional Materials in Photodetection: Mechanisms and Methodology. *ACS Nano* **2014**, *5*, 4133−4156.

(4) Li, J.; Niu, L.; Zheng, Z.; Feng, Y. Photosensitive Graphene Transistors. *Adv. Mater.* **2014**, *26*, 5239−5273.

(5) Bube, R. H. *Photoconductivity of Solids*, 1st ed.; John Wiley & sons: New York, 1960.

(6) Rose, A. *Concepts in Photoconductivity and Allied Problems*, 1st ed.; Interscience Publishers: New York, 1963.

(7) Klekachev, A. V.; Cantoro, M.; Van der Veen, M. H.; Stesmans, A. L.; Heyns, M. M.; De Gendt, S. Electron Accumulation in Graphene by Interaction with Optically Excited Quantum Dots. *Phys. E* **2011**, *43*, 1046−1049.

(8) Konstantatos, G.; Badioli, M.; Gaudreau, L.; Osmond, J.; Bernechea, M.; de Arquer, F. P. G.; Gatti, F.; Koppens, F. H. L. Hybrid Graphene−Quantum Dot Phototransistors with Ultrahigh Gain. *Nat. Nanotechnol.* **2012**, *7*, 363−368.

(9) Sun, Z.; Liu, Z.; Li, J.; Tai, G.; Lau, S.; Yan, F. Infrared Photodetectors Based on CVD-Grown Graphene and PbS Quantum Dots with Ultrahigh Responsivity. *Adv. Mater.* **2012**, *24*, 5878−5883.

(10) Zhang, D.; Gan, L.; Cao, Y.; Wang, Q.; Qi, L.; Guo, X. Understanding Charge Transfer at PbS-Decorated Graphene Surfaces toward a Tunable Photosensor. *Adv. Mater.* **2012**, *24*, 2715−2720.

(11) Huang, Y. Q.; Zhu, R. J.; Kang, N.; Du, J.; Xu, H. Q. Photoelectrical Response of Hybrid Graphene−PbS Quantum Dot Devices. *Appl. Phys. Lett.* **2013**, *103*, No. 143119.

(12) Guo, W. H.; Xu, S. G.; Wu, Z. F.; Wang, N.; Loy, M. M. T.; Du, S. W. Oxygen-Assisted Charge Transfer Between ZnO Quantum Dots and Graphene. *Small* **2013**, *9*, 3031−3036.

(13) Son, D. I.; Yang, H. Y.; Kim, T. W.; Park, W. I. Photoresponse Mechanisms of Ultraviolet Photodetectors Based on Colloidal ZnO Quantum Dot−Graphene Nanocomposites. *Appl. Phys. Lett.* **2013**, *102*, No. 021105.

(14) Cheng, S. H.; Weng, T. M.; Lu, M. L.; Tan, W. C.; Chen, J. Y.; Chen, Y. F. All Carbon-Based Photodetectors: An Eminent Integration of Graphite Quantum Dots and Two Dimensional Graphene. *Sci. Rep.* **2013**, *3*, 2694.

(15) Zheng, K.; Meng, F.; Jiang, L.; Yan, Q.; Hng, H. H.; Chen, X. Visible Photoresponse of Single-Layer Graphene Decorated with TiO_2 Nanoparticles. *Small* **2013**, *9*, 2076−2080.

(16) Kang, C. O.; Lee, S. K.; Choe, S.; Lee, Y. G.; Lee, C. L.; Lee, B. H. Intrinsic Photocurrent Characteristics of Graphene Photodetectors Passivated with Al_2O_3. *Opt. Express* **2013**, *21*, 23391−23400.

(17) Yu, W. J.; Liu, Y.; Zhou, H.; Yin, A.; Li, Z.; Huang, Y.; Duan, X. Highly Efficient Gate-Tunable Photocurrent Generation in Vertical Heterostructures of Layered Materials. *Nat. Nanotechnol.* **2013**, *8*, 952−958.

(18) Zhang, W. J.; Chuu, C. P.; Huang, J. K.; Chen, C. H.; Tsai, M. L.; Chang, Y. H.; Liang, C. T.; Chen, Y. Z.; Chueh, Y. L.; He, J. H.; Chou, M. Y.; Li, L. J. Ultrahigh-Gain Photodetectors Based on Atomically Thin Graphene-MoS_2 Heterostructures. *Sci. Rep.* **2014**, *4*, 3826.

(19) Roy, K.; Padmanabhan, M.; Goswami, S.; Sai, T. P.; Kaushal, S.; Ghosh, A. Optically Active Heterostructures of Graphene and Ultrathin MoS_2. *Solid State Commun.* **2013**, *175*, 35−42.

(20) Roy, K.; Padmanabhan, M.; Goswami, S.; Sai, T. P.; Ramalingam, G.; Raghavan, S.; Ghosh, A. Graphene−MoS_2 Hybrid Structures for Multifunctional Photoresponsive Memory Devices. *Nat. Nanotechnol.* **2013**, *8*, 826−830.

(21) Chen, S. Y.; Lu, Y. Y.; Shih, F. Y.; Ho, P. H.; Chen, Y. F.; Chen, C. W.; Chen, Y. T.; Wang, W. H. Biologically Inspired Graphene−Chlorophyll Phototransistors with High Gain. *Carbon* **2013**, *63*, 23−29.

(22) Jeon, E. K.; Yang, C. S.; Shen, Y. F.; Nakanishi, T.; Jeong, D. S.; Kim, J. J.; Ahn, K. S.; Kong, K. J.; Lee, J. O. Photoconductivity and Enhanced Memory Effects in Hybrid C60-Graphene Transistors. *Nanotechnology* **2012**, *23*, 455202.

(23) Wang, C.; Dong, H.; Hu, W.; Liu, Y.; Zhu, D. Semiconducting π-Conjugated Systems in Field-Effect Transistors: A Material Odyssey of Organic Electronics. *Chem. Rev.* **2012**, *112*, 2208−2267.

(24) Shi, Y.; Fang, W.; Zhang, K.; Zhang, W.; Li, L. J. Photoelectrical Response in Single-Layer Graphene Transistors. *Small* **2009**, *5*, 2005−2011.

(25) Xu, H.; Li, J.; Leung, B. H. K.; Poon, C. C. Y.; Ong, B. S.; Zhanga, Y.; Zhao, N. A High-Sensitivity Near-Infrared Phototransistor Based on an Organic Bulk Heterojunction. *Nanoscale* **2013**, *5*, 11850−11855.

(26) Sun, Z.; Li, J.; Yan, F. Highly Sensitive Organic Near-Infrared Phototransistors Based on Poly(3-Hexylthiophene) and PbS Quantum Dots. *J. Mater. Chem.* **2012**, *22*, 21673−21678.

(27) Sun, J.; Xiao, L.; Meng, D.; Geng, J.; Huanga, Y. Enhanced Photoresponse of Large-Sized Photoactive Graphene Composite Films Based on Water-Soluble Conjugated Polymers. *Chem. Commun.* **2013**, *49*, 5538−5540.

(28) Shrotriya, V.; Li, G.; Yao, Y.; Chu, C.; Yang, Y. Transition Metal Oxides as the Buffer Layer for Polymer Photovoltaic Cells. *Appl. Phys. Lett.* **2006**, *88*, No. 073508.

(29) Yu, Y.; Zhao, Y.; Ryu, S.; Brus, L. E.; Kim, K. S.; Kim, P. Tuning the Graphene Work Function by Electric Field Effect. *Nano Lett.* **2009**, *9*, 3430−3434.

(30) When using a light spot size that is smaller than the device dimensions (for example when using a focused laser beam), the responsivity is given by $R = (I/(P_{beam})) = [(e\lambda)/(hc)]\tau\mu V_{sd}(W/L)$, where P_{beam} is the total power of the beam.

(31) Zhang, X.; Huisman, E. H.; Gurram, M.; Browne, W. R.; Van Wees, B. J.; Feringa, B. L. Supramolecular Chemistry on Graphene Field-Effect Transistors. *Small* **2014**, *10*, 1735−1740.

(32) Zomer, P. J.; Dash, S. P.; Tombros, N.; Van Wees, B. J. A Transfer Technique for High Mobility Graphene Devices on Commercially Available Hexagonal Boron Nitride. *Appl. Phys. Lett.* **2011**, *99*, No. 232104.

(33) Note that position of the charge neutrality point for the high transit time devices (CVD graphene on silicon dioxide) lies at a substantially higher gate voltage than for the low transit time devices (mechanically exfoliated graphene on BN). The characteristics of the CVD graphene-based devices is affected by the surface traps at the silicon dioxide surface. Similar behavior was also reported in reference 31.

DOI: 10.1021/acsami.5b00610
ACS Appl. Mater. Interfaces 2015, 7, 11083−11088